ChemComm

Accepted Manuscript

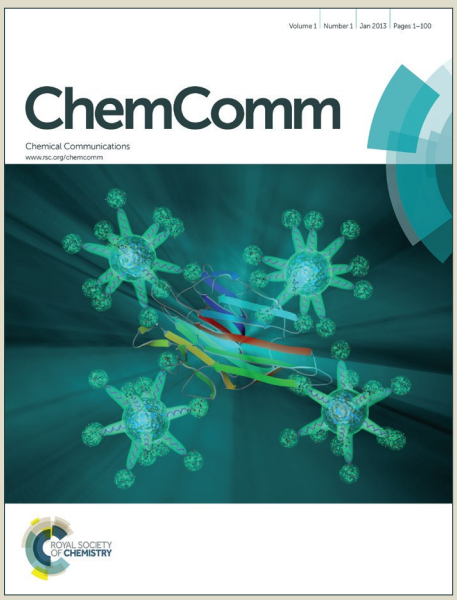

ROYAL SOCIETY OF CHEMISTRY

www.rsc.org/chemcomm

Cite this: DOI: 10.1039/c0xx00000x

www.rsc.org/xxxxxx

ARTICLE TYPE

Hierarchically porous anatase TiO_2 coated-WO_3 2D IO bilayer film and photochromic properties

Hua Li,[ab] Huazhong Wu,[c] JiajiaXiao,[b] YanliSu,[b] Jacques Robichaud,[a] Ralf Brüning,[d] and Yahia Djaoued*[a]

Received (in XXX, XXX) Xth XXXXXXXXX 20XX, Accepted Xth XXXXXXXXX 20XX

DOI: 10.1039/b000000x

A hierarchically porous anatase TiO_2 coated-WO_3 2D inverse opal (IO) bilayer film was fabricated on ITO glass using a layer by layer route with a hierarchically porous TiO_2 top layer and an ordered super-macroporous WO_3 2D IO bottom layer. This novel TiO_2 coated-WO_3 2D IO bilayer film was evaluated for photochromic applications.

In recent years, there has been much interest in inorganic photochromic materials due to their promising applications in display, imaging, and solar energy conversion[1,2]. Transition-metal oxides, such as WO_3, TiO_2, MoO_3, show color change on exposure to either sunlight or UV irradiation. Photochromism of WO_3 has attracted widespread interest. However, as a wide bandgap semiconductor, WO_3 has a short life expectancy and shows poor photochromic properties, reacting to UV light only (λ<380 nm). In order to increase its photochromic response, researchers have developed various routes, such as cathode activation[3], coupling with a narrow bandgap semiconductor[4] or with a noble metal[5]. Among these routes, coupling with TiO_2 nanoparticles attracted much attention since nano-TiO_2 greatly increases the photochromic properties of WO_3[6,7].

In order to extend the absorption of TiO_2 from UV to the visible light region, many methods[8-11] were developed, such as impurity doping[12,13] or coupling with semiconductors[14-16]. Unfortunately, whatever the kind of doping, it was found that there is a critical doping concentration which limits the efficiency of such photochromic devices[13]. Coupling TiO_2 with semiconductors of different energy level requires good matching of the conduction band and valence band of the two semiconductors[14,17]. If TiO_2 is coupled with a dye sensitizer, then high porosity and surface area are important for the sensitizer to be sufficiently adsorbed and for the paths of electron transport to be electronically interconnected[18-20].

In this communication, we present a novel designed bilayer film coupling WO_3 and TiO_2 with a highly developed porous structure. In such materials, the ordered 2D WO_3 IO functions as both coupling semiconductor and modifier of the absorption bands of a dye sensitizer, while the hierarchically porous TiO_2 coating provides an efficient area for the adsorption of the sensitizer and paths for electron transport. Such a bilayer film, for which the main steps of the fabrication procedure are illustrated schematically in Figure 1, exhibits good photochromic properties.

In previous works, following the air-water interface method, sodium dodecylsulfate (SDS) solution at 2 % was used to facilitate the PS spheres self-assembly on the surface of water[21,22]. On the other hand, it is known that the efficiency of a photochromic device is dependent on a highly crystallized dielectric material[15]. Unfortunately, the presence of cation impurities such as Na^+ from SDS is known to hinder the crystallization of the dielectric material. For example, tungsten could crystalize to Na_2WO_4 instead of WO_3, deteriorating the intercalation/deintercalation properties of a device (see ESI, Figure S1).

In order to avoid the undesired effects of the SDS surfactant on both the synthesis and the photochromic properties of the devices, a novel method was brought forward by combining aspects of the vortical surface method[23] with the air-water interface method[24]. Consequently, in this work, the 2D PS opal film was self-assembled without the use of a surfactant within a Teflon ring[23] (6 cm in diameter) floating at the surface of water. In such a process, once the 2D PS opal film is self-assembled, the water is exchanged until the solution under the PS opal becomes clear. Subsequently, a WO_3 ethanol/aqueous solution is injected under the PS opal. WO_3 penetrates into the interstitial spaces between the PS spheres from below. Then an ITO glass substrate is inserted under the floating film and the solution is slowly sucked out to deposit the PS/WO_3 opal composite monolayer onto the ITO substrate.

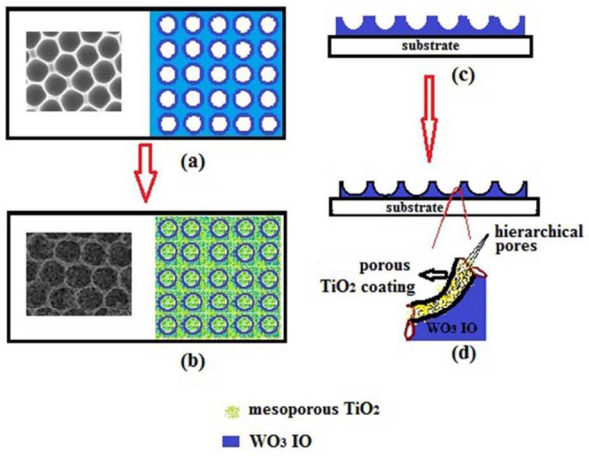

Figure 1 Schematic representation of the main steps in the fabrication of hierarchically porous anatase TiO_2 coated-WO_3 2D IO composite bilayer film. (a) & (c) WO_3 2D IO film was prepared by wet-injection strategy. (b) & (d) hierarchically porous TiO_2 was coated onto the WO_3 2D IO.

A WO_3 IO film is obtained (Figure 1a and 1c) by the removal of the PS spheres. After heating to assure good adhesion between the WO_3 IO and the ITO substrate, a TiO_2 precursor colloidal solution is used to dip-coat onto the WO_3 2D IO. A final hierarchically porous anatase TiO_2 coated on the WO_3 2D IO is obtained after calcination and burning of the P123 template (see experimental details in ESI). Figures 2 and 3 show hierarchically porous anatase TiO_2 coated-WO_3 2D IO bilayer films templated from 500 and 750 nm PS spheres, respectively, as well as the results after the intermediate fabrication steps. A clean honeycomb structure with smooth bottom is evident in the WO_3 2D IO (Figures 2(d) and 3(d)). The honeycomb structure has circular upper-end openings which give us the chance to coat another layer onto it without destroying the array structure. After coating with TiO_2, the bilayer films have a porous internal surface within the honeycomb macropores (Figures 2 (a) and 3(a)). The pores of the TiO_2 layer are around 10-100 nm in diameter (Figures 2(a), 3(a), and S2). Their hierarchical structure has a BET surface area of 125 m^2/g and a BJH pore volume of 0.34 cm^3/g (Figure S3).

The dip-coating parameters are crucial in the present experiment. When the withdrawing speed was as slow as 60 mm/min, the TiO_2 coating became too thick, hiding the 2D macropore array structure of the WO_3 2D IO monolayer (Figure S4). A 75 mm/min withdrawal speed, was the appropriate speed to obtain the TiO_2 hierarchically porous coating and keep the WO_3 2D IO structure. From the cross sectional view (Figure S5 left), one can see that the thickness of the bilayer film templated from 500 nm PS spheres is around 380 nm, with 150 nm at the bottom of the cavity left by the removal of the PS spheres. This cavity is approximately 230 nm deep. The width of the macropore is around 450 nm in diameter and its wall is around 50 nm thick. Corresponding EDS analysis (Figure S5 right) shows that the molar ratio of Ti to W is around 0.46.

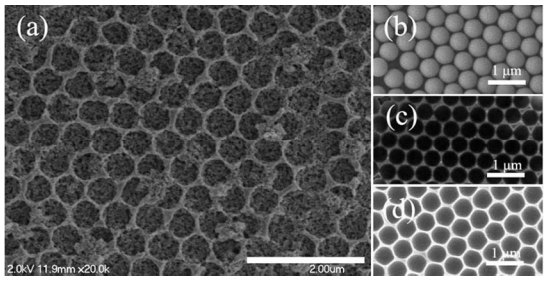

Figure 2 SEM images of hierarchically porous anatase TiO_2 coated-WO_3 2D IO composite bilayer (WT500) (a); PS opal (b); WO_3/PS composite film (c); and WO_3 2D IO (d) templated by 500 nm PS spheres.

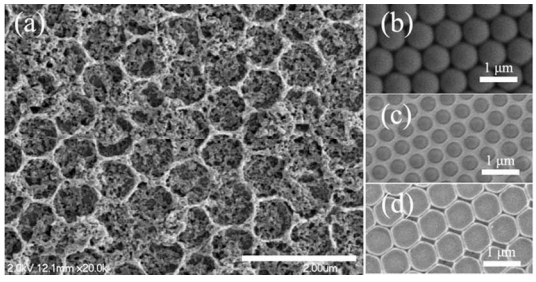

Figure 3 SEM images of hierarchically porous anatase TiO_2 coated-WO_3 2D IO composite bilayer (WT750) (a); PS opal (b); WO_3/PS composite film (c); and WO_3 2D IO (d) templated by 750 nm PS spheres.

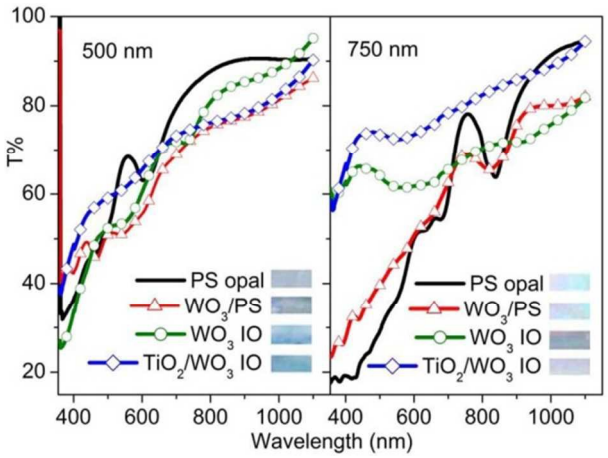

Figure 4 UV-vis-NIR transmittance spectra of PS opal films (solid line), WO_3/PS opal composite films (triangles), WO_3 IO films (circles) and TiO_2 coated-WO_3 2D IO composite bilayer (diamond) prepared from the PS spheres of 500 nm (left) and 750 nm (right). Insets show the optical reflection images from PS opal, PS/WO_3 opal composite, WO_3 IO films, and TiO_2 coated-WO_3 2D IO composite bilayer on ITO substrates.

Figure 4 shows the UV-vis-NIR transmittance spectra of PS opal, WO_3/PS opal composite, annealed WO_3 IO monolayers and TiO_2 coated-WO_3 2D IO composite films prepared, along with their corresponding optical reflection images (see Figure 4 insets). The different colors depend on the wavelength absorbed by the photonic bandgap. All the films templated from 500 nm PS spheres, show a blue color. In contrast, colors of the films templated from 750 nm PS spheres changed from pale blue to violet.

Figure S6 shows the XRD patterns of the TiO_2 coated-WO3 IO composite films templated from 500 and 750 nm PS spheres, along with the TiO_2-WO_3 composite powder obtained by scraping the film templated from 500 nm PS spheres from the substrate. The tungsten oxide peaks in the WO_3-TiO_2 composite samples are identified as monoclinic-WO_3 (pdf#43-1035, vertical solid bars). TiO_2 in the anatase form is also present (dotted vertical bars, pdf#21-1272). In order to determine the lattice parameters *a*, *b*, and *c*, a series of Gaussian peaks, superimposed on an overall quadratic background, were fitted to the experimental diffraction pattern. The peak width Δq, assumed to be the same for all reflections, is treated as a fitting parameter. After correction for the instrumental resolution, this width is used to estimate the crystallite size using the Scherrer method, with the assumption that crystallite to crystallite variations of the lattice parameter do not contribute to the peak width. The summary of XRD measurements on our samples is reported in Table S1. The average crystallite sizes are 22.4 ± 1.7 nm for m-WO_3 and 9.2 ± 0.7 nm for anatase TiO_2.

The Raman spectra (Figure S7) of the TiO_2 coated-WO_3 2D IO composite films show peaks at 806, 713 cm^{-1} (ν(O-W-O)), 326, 273 cm^{-1} (δ(O-W-O)), 136, 82.4, 73 cm^{-1} (lattice modes), which are characteristic features of the monoclinic tungsten oxide (m-WO_3).

The mode emerging at 148.6 cm^{-1} is due to the crystallization of the TiO_2 in the anatase form. This anatase main band is high-frequency shifted and broadened with respect to the single-crystal

spectrum, indicating that the TiO_2 is constituted of nanoparticles. The broadening and blue shift of the anatase main Raman band is due to a dimensional effect such as phonon confinement[25]. This phenomenon consists in the breakdown of the phonon momentum selection rule $q \cong 0$. This rule, true for Raman scattering in ordered systems, is no longer valid in the case of crystals of very small size. As the phonons are confined in space, their plane wave character is lost and all the phonons over the Brillouin zone will contribute to the first order Raman spectra. The weight of the off-center phonons increases as the crystal size decreases, and the phonon dispersion causes an asymmetrical broadening and the shift of the Raman peaks[25]. A simple confinement model may then be used to calculate the shape of the anatase main Raman mode for various nanocrystal sizes. The anatase main Raman peak is centred at 148.6 cm^{-1} (the bulk value being 144 cm^{-1}) with a full width at half maximum (FWHM) of 13.4 cm^{-1} (7 cm^{-1} being the bulk value) which corresponds to a crystal size of 9.9 nm, in agreement with the XRD results discussed above. The present result indicates that TiO_2 is well crystallized at 400 ^oC, even though previous work suggest that the crystallization of TiO_2 is inhibited when it is coupled to WO_3, even when annealed above 450 ^oC [26, 27].

The HRTEM of the TiO_2-WO_3 IO composite film templated from 750 nm PS spheres was performed on a small amount of powder obtained by scraping off the film from the substrate (Figure S8). The lattice spacings determined from the Fourier transforms of the HRTEM fringes pattern in Fig. S8(a), d = 0.39 nm, corresponds to the 002 lattice planes of m-WO_3 (pdf#43-1035). In Figure S8(b), the spacings at different points are 0.35 and 0.19 nm, assigned to the 101 and 200 lattice plane reflections of the anatase TiO_2 phase (pdf#21-1272). From the HRTEM images, the average crystallite sizes are around 20 nm for WO_3 and 9 nm for TiO_2, in agreement with the XRD results

The obtained hierarchically porous anatase TiO_2 coated-WO_3 2D IO composite bilayer film template from 750 nm PS spheres, sensitized with a ruthenium based dye, was used as active electrode in the construction of a photochromic device (named WT750)[15]. For comparison purposes, a device (named WT) was

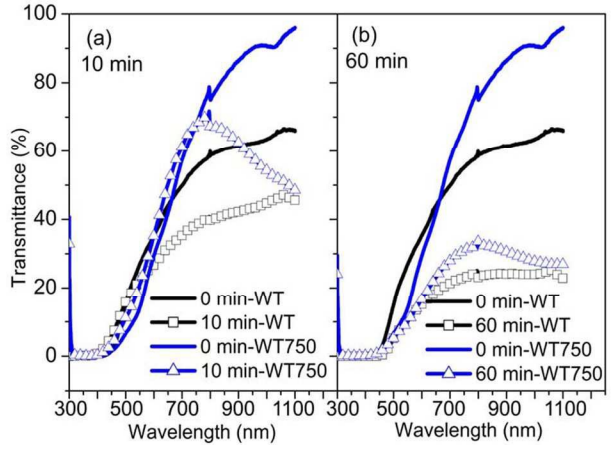

Figure 5 Photochromic response of the devices based on dye sensitized conventional TiO_2-WO_3 composite film, WT (black line); hierarchically porous anatase TiO_2 coated-WO_3 2D IO composite bilayer film, WT750 (blue line) under irradiation of 1 sun at time t=0 min, 10 min (a) and 60 min (b).

Table 1 Photochromic optical modulation

Sample	Time (min)	T (%) at 700 nm	T (%) at 1100 nm	△T (%) at 700 nm *	△T (%) at 1100 nm *
WT	0	49.9	65.9		
	10	35.4	45.5	14.5	20.4
	60	21.3	22.8	28.6	43.1
WT750	0	57.5	96.0		
	10	61.0	48.5	-3.5	47.5
	60	28.0	26.9	29.5	69.1

∗**△T** (%) = T % at 0min– T % at 10 min or 60 min.

fabricated in a similar way from a conventional TiO_2-WO_3 composite film with the same molar ratio (0.46) as the TiO_2 coated-WO_3 2D IO composite bilayer film (see ESI, Photochromic device fabrication). When light (1 sun) is incident on the surface of the device, a dye molecule absorbs a photon. Then an electron is injected from the excited state of the dye into the conduction band of TiO_2, and it diffuses into WO_3. Ionized dye molecules are reduced by I^- in the ion conducting layer (ICL) according to the reaction: $3I^- \rightarrow I_3^- + 2\,e^-$. Li ions ($Li^+$) from the ICL also diffuse into WO_3 to compensate the charge. Because of the injection of electrons, the WO_3 is reduced and its color changes from transparent to dark according to the reaction:

$$\underset{\text{transparent}}{WO_3} + xLi^+ + xe^- \leftrightarrow \underset{\text{dark}}{Li_xWO_3}$$

As the above reaction is reversible, when another ITO coated glass electrode is applied on the top of the ICL, the device is bleached when a small potential (1.0 – 3.0) is applied[15, 28].

Figure 5 and Table 1 present the photochromic optical modulations of the fabricated devices. In the first 10 min, WT750 showed a higher absorption contrast (47.5 %) than WT (34.0 %) in the NIR 1100 nm. At 700 nm (Vis) WT750 showed negligible contrast (-3.5%), while WT exhibits a contrast of 10%. The high absorption in NIR range compares favourably with a photochromic device based on mesoporous TiO_2/WO_3 composite bilayer film reported by Djaoued *et al.*[15], in which the absorption contrast at 1100 nm was around 25 % after 10 min irradiation. At t = 60 min, the WT750 device shows an outstanding absorption contrast of 69.1 % at 1100 nm in comparison with WT, which only has an absorption contrast of 38.2 %. Further, after 60 min irradiation, in the visible region, there is nearly the same absorption contrast between WT750 and WT. The present result of 42 % absorption contrast at 800 nm after 60 min irradiation for WT750, exceeds the 25 % contrast reported by Huang et al. for $TiO_{2-x}N_x$/$Ni(OH)_2$[7]. Therefore, the absorption takes place mainly in the NIR range, while allowing the visible light to pass through. This remarkably high transmittance response in the NIR region of the WT750 device is attributed to the hierarchically porous structure, the well crystallized anatase TiO_2, and the good coupling of TiO_2 with the highly ordered macroporous structure of the WO_3 2D IO. Hence, this device qualifies for smart window application.

Conclusions

Hierarchically porous anatase TiO_2 coated-WO_3 2D IO composite bilayer films on ITO substrate, templated from 500 nm and 750 nm PS spheres, were designed and prepared using a layer by layer

route. Ideas were borrowed from the 'vortical surface method' and 'air-water interface method' to develop a new procedure to prepare the WO_3 2D IO bottom layer. Dip-coating was used to produce the TiO_2 top layer.

The films featured a hierarchically porous TiO_2 structure with pores from 10 to 100 nm and homogeneous macropores inherited from the WO_3 2D IO. Such bilayer films show a well crystallized anatase TiO_2 top layer with an m-WO_3 under layer, which is favourable for fabrication of a photochromic device. The novel device was evaluated for prospective use in smart window applications with a high absorption in NIR range and mild absorption in the visible region.

ACKNOWLEDGEMENTS. The financial support of National Natural Science Foundation of China (grant No.21301123), the National Science and Engineering Research Council (NSERC) of Canada, the John R. Evans Leaders Fund of Canada Foundation for Innovation (CFI), and of the Research Assistantships Initiative of New Brunswick Innovation Fund (NBIF) is gratefully acknowledged. We also greatly thank the help in micro-Raman characteristic from Tianjin Gangdong SCI&Tech. Development Co. LTD.

Notes and references

[*a] *Corresponding Author, Laboratoire de Recherche en Matériaux et Micro-spectroscopies Raman et FTIR, Université de Moncton-Campus de Shippagan, Shippagan, NB, E8S1P6, Canada. Fax: +1506 336 3434; Tel: +1506 336 3412; E-mail: *Corresponding Author, Yahia Djaoued, Yahia.djaoued@umoncton.ca*

[b] *Department of Inorganic Materials, College of Chemistry Chemical Engineering and Materials Science, Soochow University, 199 Renai Road, Suzhou 215123, Jiangsu Province, PR China,*

[b] *Department of Chemistry and Chemical Engineering, MinJiang University, Fuzhou, Fujian Province 350108, PR China*

[c] *Department of Chemistry and Chemical Engineering, MinJiang University, Fuzhou, Fujian Province, 350108, PR China*

[d] *Physics Department, Mount Allison University, Sackville, NB, E4L1E4, Canada*

† Electronic Supplementary Information (ESI) available: [Experimental details; figures including SEM, Raman, XRD, HRTEM]. See DOI: 10.1039/b000000x/

1 S. Songara, M. K. Patra, M. Manoth, L. Saini, V. Gupta, G. S. Gowd, S. R. Vadera and N. Kumar, *Journal of Photochemistry and photobiology A: Chemistry*,2010, **209**, 68.

2 B. Chi, L. Zhao, T.Jin, *J. Phys. Chem. C,* 2007, **111**, 6189.

3 J. N. Yao, K. Hashimoto, K. Hashimoto, A. Fujishima, *Nature*, 1992, **355**, 624.

4 (a) J. C. Santato, M. Ulmann, J. Augustynski, *Adv. Mater.*, 2001, **13**, 511; (b) M. A. Quevedo-Lopez, R. Ramirez-Bon, R. A. Orozco-Teran, O. Mendoza-Gonzalez, *Thin Solid Film*, 1999, **343**, 202.

5 T. He, Y. Ma, Y. A. Cao, P. Jiang, W. S. Yang, J. N. Yao, *Langmuir*, 2001, **17**, 8024.

6 (a) T. He, Y. Ma, Y. A. Cao, H. M. Liu, G. J. Zhang, W. S. Yang, J. N. Yao, *J. Phys. Chem. B*, 2002, **106**, 12670; (b) M. J. Taylor, *Phys. Lett. A*, 1968, **27**, 32.

7 H. Huang, S. X. Lu, W. K. Zhang, Y. P. Gan, C. T. Wang, L. Yu, X. Y. Tao, *Journal of Physics and Chemistry of Solids*, 2009, **70(3-4)**, 745.

8 Y. Pang, W. Feng, J. Chen, Y. Liu, W. Cai, *J. Mater. Sci.Technol.,* 2007, **23**, 477.

9 D. Kaczmarek, J. Domaradzki, A. Borkowska, *Thin Solid Films,* 2007, **515**, 6347.

10 Y. Zhang, X. Xiong, Y. Han, X. Zhang, F. Shen, S. Deng, H. Xiao, X. Yang, G. Yang, H. Peng, *Chemosphere,*2012, **88,** 145.

11 Q. Li, J. K. Shang, *J. Am. Ceram. Soc.*, 2008, **91(2)**, 660.

12 S. U. M. Khan, M. Al-Shahry, W. B. Jr. Ingler, *Science,* 2002**, 297**, 2243.

13 (a) C. He, Y. Yu, X. Hu, A. Larbot, *Appl. Surf. Sci.,* 2002, **200**,239. (b) C. M. Teh, A. R. Mohamed, *J. Alloys Compd.,* 2011, **509**, 1648.

14 H. Zhang, G. Chen, D. W. Behnemann, *J. Mater. Chem.*, 2009, **19**, 5089.

15 Y. Djaoued, S. Balaji, N. Beaudoin, *J Sol-Gel Sci.Technol.,* 2013, **65(3)**, 374.

16 S. Kuang, L. Yang, S. Luo, Q. Cai, *Appl. Surf. Sci*., 2009, **255**, 7385.

17 R. Daghrir, P. Drogui, D. Robert, *Ind. Eng. Chem. Res.,* 2013, **52(10)**, 3581.

18 E. S. Kwak, W. Lee, N.-G. Park, J. Kim, H. Lee, *Adv. Funct. Mater.,* 2009,**19,** 1093.

19 M. J. Cass, A. B. Walker, D. Martinez, L. M. Peter, *J. Phys. Chem. B,* 2005, **109**, 5100.

20 P. Wang, S. M. Zakeerudin, J. d E. Moser, M. K. Nazeeruddin, T. Sekiguchi, M. Gratzel, *Nat. Mater.,* 2003,**2**, 498.

21 J. Yu, Q. Yan, D. Shen, *ACS Appl. Mat. Inter.*, 2010, **2**, 1922.

22 H. Li, G. Vienneau, M. Jones, B. Subramanian, J. Robichaud, Y. Djaoued, *J. Mater. Chem. C*, 2014, **2**, 7804

23 F. Pan, J. Zhang, C. Cai, T. Wang, *Langmuir*, 2006, **22(17)**, 7101.

24 J. Yu, Q. Yan, D. Shen, *Applied Materials & Interfaces,* 2010, **2(7)**, 1922.

25 S. Balaji, Y. Djaoued, J. Robichaud, *J. Raman Spectrosc.,* 2006, **37**, 1416.

26 L E. Depero, IN.Sora, C. Perego, L. Sangaletti, G. Sberveglieri, *Sens Actuators B,* 1996, **31**, 19.

27 UO. Krasovec, A.Georg, A. Georg, V. Wittwer, J. Luther, *Sol Energy Mater Sol Cells,* 2004, **84**, 369.

28 S.Balaji, Y.Djaoued, A.-S. Albert, R. Bruning, N. Beaudoin,J. Robichaud, J. Mater. Chem.,2011, **21**, 3940.